Title
Continuum simulation of dislocation dynamics: Predictions for internal friction response

Journal
Computational Materials Science, 25(3)

Authors
Greaney, P. Alex
Friedman, Lawrence H.
Chrzan, D.C.

Publication Date
2002-02-19

Continuum Simulation of Dislocation Dynamics: Predictions for Internal Friction Response

P. Alex Greaney, Lawrence H. Friedman,* and D. C. Chrzan

Department of Materials Science and Engineering, University of California Berkeley, CA 94720 and Center for Advanced Materials Materials Sciences Division Ernest Orlando Lawrence Berkeley National Laboratory Berkeley, CA, 94720

(Dated: February 19, 2002)

Abstract

The amplitude dependent mechanical loss due to bowing of an idealized Frank-Read Source is studied using both simulation and analytical techniques. Dislocations are modeled within isotropic elasticity theory, and are assumed to be in the over-damped limit. The dynamics incorporated in the model are tested directly, by comparison with the exact solution to the linearized isotropic elasticity theory of the mechanical losses. The model is then applied to the study of the mechanical losses from two coupled dislocations. It is concluded that the implemented dislocation dynamics method represents an accurate solution to the intially stated problem, that the elastic string model often employed to model losses is inadequate, and that dislocation interactions may alter substantially the dislocation component of the spectrum observed during internal friction experiments.

PACS numbers:

*Currently at University of Groningen, Netherlands Institute for Metals Research, Applied Physics Micromechanics Group, Nijenborgh 4 9747 AG Groningen, The Netherlands.

I. Introduction

There are a number of efforts worldwide aimed at computing the dynamic evolution of collections of dislocations with the long term goal of predicting mechanical properties [1–10]. To achieve this long term goal, dislocation simulations must provide an adequate representation of the purported physics, and the physical assumptions implied by the simulations must be verified. Thus, during the current period of rapid dislocation simulation development, it is necessary both to use dislocation dynamic simulations to advance understanding of mechanical properties while at the same time to demonstrate their validity.

Initial efforts to validate dislocation simulations and to exploit their predictive power focused attention on final dislocation structures [3, 9–12]. Later work emphasizes more the dynamics of collections of dislocations [5, 13].

When resulting dislocation structures are used to validate a dislocation model, the dynamics of a population of dislocations are simulated, and the computed structures are compared with experimentally observed patterns. However, one of the primary difficulties in developing a theory of the formation and evolution of dislocation structures is that many different theories may yield similar structures. Therefore, the task becomes not to model dynamics that generate patterns similar to those observed experimentally, but rather to insure that the physics underlying the pattern formation is the same in both the experiment and the theory. A direct comparison of the modelled dynamics of interacting dislocations to experimental observations helps to establish this similarity.

Often, this comparison is done by simulating the constant strain rate response of a material (see for example [13]). A favorable comparison offers some evidence that the simulated dislocation dynamics are similar to those underlying the results of experiment. However, modeling of a constant strain rate test starting with dislocation dynamics involves a significant level of "coarse graining," and the final comparison is insightful only insofar as the coarse grained result is sensitive to small scale details.

Mechanical spectroscopy experiments [14] offer an additional check for theories of dislocation dynamics. In a typical experiment, a bias stress is applied to the sample, and small amplitude oscillatory (in time) stress is superimposed. The work done by the oscillatory stress is a measure of the loss. These experiments are particularly attractive, because they probe dislocation dynamics directly. The experimental mechanical loss as a function of

frequency can be directly compared with the loss predicted by simulations of dislocation structures; however, similar to comparisons with constant strain rate experiments, this comparison provides a stringent check only if the assumed model for the mechanical losses is really capable of describing the experimental situation. This comparison is confounded by the fact that experiments measure the response from many loss mechanisms simultaneously. Hence experiments must be designed carefully in order to evaluate the contributions from glide of the dislocations as opposed to other other loss mechanisms, for example, dislocation climb or diffusion of solutes.

One must also insure that dislocation dynamics simulations are a good representation of dislocations within elasticity theory. The quality of this representation should not be taken for granted, but rather, should be checked whenever possible by direct comparison with *exactly* solved problems in the dynamics of dislocations governed by elasticity theory. A common test, for example, is to calculate the operation stress of a Frank-Read source.

An additional check is presented here. The small stress amplitude mechanical loss problem is solved analytically, and the results then used to validate the dislocation dynamics simulations. Because the dislocation dynamics simulation has been so validated, its use can be confidently extended to probe other regimes of mechanical loss, such as large amplitued losses and mechanical losses stemming from two interacting dislocation segments.

In these studies, it is demonstrated that the elastic string model proposed by Granato and Lücke [15] is sometimes an inadequate model for the losses. Further, it is demonstrated that dislocation interactions exert a large influence on the resulting losses. Hence simple models for mechanical losses that rely on the response of isolated dislocations are probably inadequate descriptions of the losses from dislocation structures.

The remaining sections are organized as follows. Section II of this manuscript describes briefly the computer model employed, as well as a test of the accuracy of the force computation scheme. Section III provides an introduction to the physical problem, but the discussion is limited to low amplitude oscilliatory stresses in the absence of a bias stress. In this limit, an exact solution is obtained for the mechanical losses. The exact solution is then compared with the predictions of dislocation dynamics simulations and the predictions of the Granato-Lücke model for the losses. Section IV treats a number of more general cases, including large amplitude stress oscillations and the presence of non-oscillating bias stresses that are often applied in experiments. Section V discusses mechanical losses stemming from

two interacting dislocations segments. Section VI contains the conclusions, section VII the acknowledgments, and section VIII a mathematical appendix.

II. Computer Model

A previously developed model [16, 17] is adapted to simulate the mechanical loss response of simple dislocation structures. In this model, dislocations are described by isotropic elasticity theory and are presumed to be contained in an infinite homogeneous medium. The simulation accounts for the full stress state due to all dislocations considered. The dynamic behavior of the dislocation is assumed to be in the over-damped limit and governed by a linear drag law. Radiation and inertial effects are neglected. The drag coefficient is assumed to be independent of dislocation velocity and orientation.

These assumptions are most appropriate for simulatings dislocations in materials with low Peierls barriers, at temperatures above the Debye temperature, and when loading frequencies are sub-GHz. The parameters are chosen, therefore, to represent Al: A Burgers vector of magnitude $b = 2.86$ Å, a shear modulus of $\mu = 26.5$ GPa, a drag coefficient of $B = 0.08$ Pa-s, a Poisson's ratio of $\nu = 0.347$, and the dislocation is treated as if undissociated. The small scale cutoff procedure employed by Hirth and Lothe [18] is applied, and the cutoff is chosen to be (except where noted) $\rho = b/3$.

The simulation decomposes the dislocation into segments extending between points. The points are indexed by the subscript i and the vector $\hat{\mathbf{u}}_i$ indicates the glide direction normal to the dislocation line direction at point i. The velocity of the ith point is given by

$$\frac{\partial \mathbf{u}_i}{\partial t} = \frac{(((\boldsymbol{\sigma}_i \cdot \mathbf{b}) \times \boldsymbol{\xi}_i) \cdot \hat{\mathbf{u}}_i)\, \hat{\mathbf{u}}_i}{B}. \tag{1}$$

Where $\boldsymbol{\xi}_i$ and $\boldsymbol{\sigma}_i$ are the line direction and stress at the ith point, $\mathbf{b}$ is the burgers vector. The stress felt by the ith dislocation point, $\boldsymbol{\sigma}_i$, reflects the contributions from the applied stress as well as the self-stress of the dislocation and the stress from all other dislocations in the solid. Equations (1) are integrated using an adaptive step size fourth order Runge-Kutta integration scheme. This approach is described fully in reference [16].

A dislocation configuration typical of those considered here is shown in figure 1. Only dislocation segments lying in the $z = 0$ plane are mobile. The corners of the dislocations are assumed fixed.

The force on each of the points is composed of two contributions: A contribution from the segments nearest to the point in question, and the contributions form all further segments. The nearest neighbor contributions are computed by assuming the dislocation arc passing through three adjacent points is part of a circular arc, and computing the exact contribution to the stress on the point in question. The contributions from segments further away are computed by assuming that linear dislocation segments are connecting each of the defined dislocation points.

The presence of corners in our dislocation configurations requires further approximation. Isotropic elasticity theory predicts that stress fields near dislocations "corners" (*e. g.* the ends of cross-slipped segments) become infinite. These infinite stresses are treated using a cutoff scheme described below. Nevertheless, even with the cutoff, the corner-stresses will remain quite large, and one expects that the corners will not remain atomically sharp. Motion at or near corners is therefore non-conservative. Unfortunately, the extent to which corners round is difficult to ascertain from existing calculations. Consequently, it is not possible to provide a well tested description of "corner" dynamics for the dislocation codes.

The current simulations do not allow the "corners" of the dislocation to be mobile. However, corners still pose difficulties. As such the code is prevented from considering points "too close" to any corner. This in turn raises the question of how close is "too close." As a working rule the small scale cutoff distance is used, but this has no physical basis. (The small scale cutoff is a distance chosen so that elasticity theory correctly calculates the total energy of a straight dislocation with out including a core energy term [23].) A rigorous treatment of corner dynamics awaits further study.

The quality of the force calculation in the code has been verified by considering the exact results for circular dislocation arcs. Figure 2b compares the exact analytical solution for the force, the calculation of the force using the model, and the predictions of a simple line tension model assuming the proper orientation dependent line tension [18]. Figure 2b indicates that the forces predicted by the scheme described here are in good agreement with the exact result for a circular arc with a diameter of 1 μm. Further, the line tension approximation employed in more simple studies can err by as much as 25%.

A more complete test of the simulation code, however, requires that one investigate directly the dynamic response of dislocations. This, in turn, requires the exact solution to a dislocations dynamics problem that can serve as a check for the simulations. This exact

solution is presented in the next section.

III. Mechanical Loss in the Low Stress-Amplitude Limit

As mentioned in the introduction, mechanical spectroscopy offers the promise of probing dislocation dynamics directly. However, the same mechanical spectroscopy experiments yield signals from a variety of loss mechanisms, and associating features of the loss spectra with specific mechanical processes is often difficult. Therefore, a direct favorable comparison of simulated loss spectra with experiment is a necessary but not sufficient test of the quality of the theory. An alternate approach is to compare the results of simulation with analytical results known to be correct.

Unfortunately, a general analytical expression for the mechanical losses expected from a dislocation within an infinite isotropic elastic medium is not available. It is demonstrated here, however, that in the limit that the amplitude of the dislocation's oscillatory motion is smaller than the small scale cutoff employed in the computation of forces, that one can obtain an analytical solution for the expected mechanical losses and dislocation configurations. While in a "real" crystal, this limit cannot be obtained (as mentioned above, the small scale cutoff for dislocation forces is typically of the order of $b/3$) it is possible to explore this regime using the dislocation dynamics model described in the previous section.

The simple dislocation configuration, of a closed rectangular loop forming a Frank-Read source, shown in figure 1, is the starting point for the calculations. Only the dislocation segment on the glide plane is glissile, and the loop is closed with a sessile segment 10μm from the slip plane. Mechanical losses from the driven dislocations are calculated according to the following procedure. A periodic stress (and later, static bias stresses) is applied to the dislocation, and the area swept out by the dislocation as a function of time is recorded. The energy loss from the dislocation is calculated according to

$$\Delta W = \left\langle \int_{\tau}^{\tau+2\pi/\omega} \sigma_a \cos(\omega t) b \frac{\partial A}{\partial t} dt \right\rangle, \tag{2}$$

where τ is a time in the "steady state"regime, ω is the angular frequency, and $\sigma_a \cos(\omega t)$ is the time dependent applied shear stress at time t. The time dependent strain from the motion of this dislocation, ε, is proportional to $A(t)$, the area swept out at time t, and the number of dislocations. The loss is taken to be proportional to the area of the area vs stress

hysteresis loop [24].

The starting point for the analysis is the equation of motion for an elemental segment of dislocation at position $\boldsymbol{r}$ and with line direction and burgers vectors $\boldsymbol{\xi}$ and $\boldsymbol{b}$.

$$B\frac{\partial \boldsymbol{r}}{\partial t} = \boldsymbol{\sigma}(\boldsymbol{r}) \cdot \boldsymbol{b} \times \boldsymbol{\xi}(\boldsymbol{r}). \tag{3}$$

Here $\boldsymbol{\sigma}(\boldsymbol{r})$ is the stress tensor at $\boldsymbol{r}$, which is the sum of the externally applied stress and the self stress from the whole dislocation.

The stress state is given by

$$\boldsymbol{\sigma}(\boldsymbol{r}) = \boldsymbol{\sigma}_a \cos(\omega t) + \boldsymbol{S}(\boldsymbol{r}), \tag{4}$$

where $\boldsymbol{\sigma}_a \cos(\omega t)$ is an externally applied sinusoidal stress and self stress is given by

$$\begin{aligned} \boldsymbol{S}(\boldsymbol{r}) \;=\; & \frac{\mu}{4\pi} \oint_{\text{line}} \left\{ (\boldsymbol{b} \times \boldsymbol{\nabla}') \frac{1}{R} \otimes d\boldsymbol{l}' \right\} \\ & + \frac{\mu}{4\pi} \oint_{\text{line}} \left\{ d\boldsymbol{l}' \otimes (\boldsymbol{b} \times \boldsymbol{\nabla}') \frac{1}{R} - \boldsymbol{\nabla}' \cdot \boldsymbol{b} \times d\boldsymbol{l}') (\boldsymbol{\nabla} \times \boldsymbol{\nabla} - \boldsymbol{I}\boldsymbol{\nabla}^2) \frac{R}{(1-\nu)} \right\}, \end{aligned} \tag{5}$$

where ν is Poisson's ratio, $d\boldsymbol{l}' = \boldsymbol{\xi}(\boldsymbol{r}')|dl'|$ (where dl is an incremental distance along the line) and $R = |\boldsymbol{r}' - \boldsymbol{r}|$ [18]. The cutoff procedure employed is the same as used by the dislocation code. Note that the statement of the problem here neglects elastic radiation effects. Instead, the stress field felt by the dislocation at any instant of time is taken to depend only on the applied stress at that time, and the current configuration of the dislocation. This approximation is most suitable at low driving frequencies.

The small amplitude approximation for the dislocation's motion is consistent with the following description of the dislocation configuration. The mobile segment of the Frank-Read source is limited to the range $0 \leq x \leq L$. This allows the glissile dislocation line to be parameterized in x giving the position of the dislocation line $\boldsymbol{r} = (x, y(x,t), 0)$. Forbidding over-bowing and pinning the ends of the dislocation allow the mobile section of dislocation line to be represented by a sine Fourier series:

$$y(x,t) = \sum_{\substack{n=1 \\ n\,\text{odd}}}^{\infty} a_n(t) \sin\left(\frac{n\pi x}{L}\right). \tag{6}$$

An exact (but frightening) expression for the force per unit length that the dislocation exerts on its self ($\boldsymbol{F}_{\text{self}}$) is obtained using the Peach-Koehler formula on the fourier repre-

sentations of the dislocation line and its line direction

$$\boldsymbol{F}_{\text{self}} = \boldsymbol{S}\left(x, \sum_{n}^{\infty} a_n(t)\sin(\frac{n\pi x}{L}), 0\right) \cdot \boldsymbol{b} \times \boldsymbol{\xi}\,(\boldsymbol{r}) \quad . \tag{7}$$

The self stress can be well approximated by the Taylor series expansion of the $\hat{\boldsymbol{y}}$ component of the $\boldsymbol{F}_{\text{ self}}$ about the equilibrium position in terms of the fourier coefficients $\{a_n\}$ if the set of fourier coefficients $\{a_n\} < \frac{n\pi}{L}$. Moreover it can be shown that the true self force is well approximated by just the first order terms in this series if the amplitudes $\{a_n\}$ are small in comparison to the elastic cutoff ρ. One can therefore neglect modes with wavelengths smaller that the elastic cut off.

When only terms first order in $\{a_n\}$ are included in the Taylor series expansion the $\hat{\boldsymbol{y}}$ component of the self force becomes the sum of force distribution functions, $f_n(x)$ for each mode in the Fourier series:

$$F_{y\ \text{self}} \approx \sum_{\substack{n=1 \\ n\,\text{odd}}}^{\infty} a_n(t) f_n(x). \tag{8}$$

The derivation of the force distribution functions and their general form are given in the appendix.

With these approximations in place the original problem can be recast as the following coupled ordinary differential equations,

$$B\sum_{\substack{n=1 \\ n\,\text{odd}}}^{\infty} \sin\left(\frac{n\pi x}{L}\right)\frac{da_n(t)}{dt} = b\sigma_a\cos(\omega t) + \sum_{\substack{n=1 \\ n\,\text{odd}}}^{\infty} a_n(t) f_n(x), \tag{9}$$

where σ_a is now the externally applied stress amplitude resolved on the slip system and ω is the angular frequency of the applied stress. Pre-multiplying by $\frac{2}{L}\sin\left(\frac{m\pi x}{L}\right)$ and integrating over $0 \le x \le L$ one finds:

$$B\dot{\boldsymbol{a}}(t) = \boldsymbol{\Gamma}\cos(\omega t) + \boldsymbol{\alpha}\cdot\boldsymbol{a}(t), \tag{10}$$

where $\boldsymbol{a}(t) = (a_1(t), a_3(t), a_5(t), \cdots)$, $\boldsymbol{\Gamma} = \frac{4\sigma_a b}{\pi}\left(\frac{1}{1}, \frac{1}{3}, \frac{1}{5}, \cdots\right)$ and the matrix $\boldsymbol{\alpha}$ is given by

$$\boldsymbol{\alpha} = \begin{pmatrix} \alpha_{11} & \alpha_{13} & \cdots \\ \alpha_{31} & \alpha_{33} & \cdots \\ \vdots & \vdots & \end{pmatrix} \tag{11}$$

with the elements

$$\alpha_{kj} = \frac{2}{L}\int_0^L dx f_j(x)\sin\left(\frac{k\pi x}{L}\right). \tag{12}$$

The set of differential equations is decoupled by finding the set of eigenvalues, $\{\lambda_n\}$, and eigenvectors, $\{\boldsymbol{\epsilon}_n\}$ of $\boldsymbol{\alpha}$ so that $\boldsymbol{\alpha}\boldsymbol{\epsilon}_n = \lambda_n \boldsymbol{\epsilon}_n$. If the vectors $\boldsymbol{a}(t)$ and $\boldsymbol{\Gamma}$ are expressed as linear combinations of the eigenvectors

$$\boldsymbol{a}(t) = \sum_{\substack{m=1 \\ m\,\text{odd}}}^{\infty} \gamma_m(t)\boldsymbol{\epsilon}_m, \tag{13}$$

$$\boldsymbol{\Gamma} = \sum_{\substack{m=1 \\ m\,\text{odd}}}^{\infty} \psi_m \boldsymbol{\epsilon}_m, \tag{14}$$

then the decoupled equations have steady state solutions of

$$\gamma_m(t) = \gamma_m^{\circ} \cos\left(\omega t + \theta_m\right), \tag{15}$$

where

$$\theta_m = \arctan\left(\frac{B\omega}{\lambda_m}\right) \tag{16}$$

and

$$\gamma_m^{\circ} = \frac{\psi_m}{\lambda_m \cos(\theta_m)\left\{\left(\frac{B\omega}{\lambda_m}\right)^2 + 1\right\}}. \tag{17}$$

Finally, the expression for the dislocation position becomes:

$$y(x,t) = \sum_{\substack{n=1 \\ n\,\text{odd}}}^{\infty} \sin\left(\frac{n\pi x}{L}\right) \sum_{\substack{m=1 \\ m\,\text{odd}}}^{\infty} \epsilon_{mn}\gamma_m^{\circ} \cos\left(\omega t + \theta_m\right) \quad . \tag{18}$$

The mechanical energy lost per cycle is obtained by integrating the total work done over the cycle, so the loss is

$$\Delta W = \int_{\tau}^{\tau + 2\pi/\omega} dt \int_0^L dx \sigma_a b \cos(\omega t) \frac{dy(x,t)}{dt}, \tag{19}$$

which becomes

$$\Delta W = -2\sigma_a b L \sum_{\substack{n=1 \\ n\,\text{odd}}}^{\infty} \frac{1}{n} \sum_{\substack{m=1 \\ m\,\text{odd}}}^{\infty} \epsilon_{mn}\gamma_n^{\circ} \sin(\theta_m) \tag{20}$$

where ϵ_{mn} is the nth component of the mth eigenvector.

In practice, to perform this calculation it is necessary to truncate the Fourier series. The proper termination point for the series is dictated by the rate of convergence. The force distribution functions, $f_n(x)$, have strong extrema at a distance of ρ from the pinned ends

of the mobile segment and then decay exponentially with distance from the pinned points. In order to get a good representation of $\{f_n(x)\}$ with a truncated Fourier series one must include all eigenfunctions down to those with wavelengths on the order of ρ. Clearly the slow convergence of the Fourier series to the $\{f_n(x)\}$ is the limiting step in summing enough terms to converge the solution (18). To obtain a fast convergence the set of $\{f_n(x)\}$ and the $\boldsymbol{\alpha}$ matrix is calculated using a large inner cutoff length, $\rho = 5 \times 10^{-9}$m ($\simeq 17\,|\boldsymbol{b}|$), and ignoring the static stress field from the sessile parts of the dislocation. This procedure does not represent a physically meaningful situation, but rather provides a result that can be tested directly in the computer simulation and consequently allows a direct check of the code's description of dislocation dynamics. (It must be noted that the amplitudes of the displacements are such that the number of the grid points remains constant throughout the entire sequence. Hence the comparison here does not provide a complete test of the dislocation discretization scheme.)

The predictions of the above analytical theory are then compared with the results of simulation and the predictions of the theory of Granato and Lücke [15]. The predictions of the simulations are computed as follows. The simple dislocation configuration of figure 1 is established (although the stresses from the arms and top closing segment are ignored), and a periodic stress is applied to the dislocation. The hysteresis loops (in the stress-area plane) of the dislocation are recorded. The simulations are run until a numerically steady state regime is reached (*i. e.* a regime in which there is no drift in the area of the hysteresis loop, within the numerical accuracy of the simulations). The steady state losses are then averaged over 8 cycles to reduce the numerical noise.

Figure 3 shows the loss spectra predicted by the Fourier series method (using the first ten terms[25]), the dislocation code and Granato-Lücke theory [26]. The bowing dislocation segment is taken to be 1 μm long, and the amplitude of the periodic driving shear stress is taken to be 0.5 MPa. The Granato-Lücke theory predicts the highest frequency of the three for the maximum losses, and also underestimates the magnitude of the maximum loss. By adjusting the segment length withing the Granato-Lücke theory, a better, but not perfect, prediction for the maximum loss as well as the position of the loss peak is obtained; however, the agreement between the analytical results and the dislocation dynamics simulations is, however, excellent. (Note that the statistical error bars associated with the simulation results are smaller than the size of the symbols used for plotting.)

The failure of the string-like line-tension treatment of the dislocation to capture the dynamics of the true dislocation (at this driving frequency) can be seen by examining the bowing configurations of dislocation during the loading cycle shown in figure 4. It can be seen that the dislocation bows out as an "m" shape, and that the dislocation nearest the pinned ends leads the bowing through the equilibrium configuration. The line-tension approximation has similar behavior, but to a much lesser extent.

IV. Losses From Isolated Dislocations

The model is now applied to the study of mechanical losses arising from simple dislocation configurations of the type shown in figure 1 with large bias and oscillatory stresses. Specifically, the dislocations move under an applied stress of

$$\boldsymbol{\sigma} = \boldsymbol{\sigma}_{\text{bias}} + \boldsymbol{\sigma}_a \cos \omega t \ , \tag{21}$$

where $\boldsymbol{\sigma}_{\text{bias}}$ is a static bias stress, and the other parameters are defined as above. In addition, the full interactions between all segments are now considered (though only the single segment is allowed to move), and the cutoff, ρ, is restored to the value $b/3$.

Driven isolated dislocation sources have two temporally stable types of behavior. One behavior is modelled well by the losses expected from a linear, damped massless oscillator. The other behavior displays a distinctly different frequency dependence for the mechanical loss.

Figure 5 shows example hysteresis loops and loss spectra for biased and unbiased, 1μm, edge and screw Frank-Read sources under an 8 MPa driving shear stress. Both linear and non-linear losses are represented in these plots. In the "linear" regime, the loss spectrum of the dislocation resembles the Lorentzian shape (see figure 5) for a 1-dimensional, massless, damped linear oscillator given by

$$\Delta W = \frac{F_a^2 \omega D}{\kappa^2 + (\omega D)^2}. \tag{22}$$

Here F_a is the applied force amplitude, κ is the oscillator stiffness, ω the angular driving frequency and D the damping coefficient. The hysteresis loops of linear behavior are elliptic, as can be see from figure 5. Although the frequency dependence of loss in this regime approximates equation (22), it is found that the parameters, κ and D, are dependent on the

bias stress, $\boldsymbol{\sigma}_{\text{bias}}$, and the cyclic stress amplitude, $\boldsymbol{\sigma}_a$. Equation (22) serves as a simple model for the losses observed during linear behavior, hence the features evident in the loss spectra are discussed below in terms of "effective stiffness" κ and "effective drag" D, and how these parameters change with the stress conditions. For now, it is noted that the maximum loss appears at a frequency given by $\omega_{\max} = \kappa/D$, and the amplitude of the loss is given by $F_a^2/(2\kappa)$. It is apparent that if one increases the value of κ, the peak is shifted to higher frequencies, and the maximum loss is reduced. Increasing the drag coefficient D simply translates the entire curve to lower frequencies. A set of normalized plots is shown in figure 6. At a 10 MPa oscillatory stress, where over-bowing occurs at low frequencies, the plot is normalized with respect to the local maxima. The origins of non-elliptic shaped hysteresis loop are now discussed in detail.

IV.A. Dynamics - Non-Linear Behavior

The "critical configuration" of a Frank-Read source is the unstable equilibrium shape of the dislocation under the homogeneous "critical shear stress," *i. e.* the stress at which the source is just able to produce a dislocation. Due to both the logarithmic dependence of the dislocation line tension on length, and the stress field from the dislocation arms extending normal to the slip plane (in the considered case), the critical configuration changes with the pinning length of the source. As the pinning length increases (with the same $\boldsymbol{b}$ and ρ) the critical shape tends toward the elliptical shape predicted by the line tension approximation.

The notion of a critical configuration is applicable only to static dislocations, as the dynamic path of a dislocation is dependent on the loading conditions. In fact, sources can be loaded cyclicly with peak stresses very much larger than their static operation stress without operating as a Frank-Read source. Considering this situation, one has the following observations. Earlier work has demonstrated that there is a stress dependent characteristic time to operate a Frank-Read source, and that this time increases rapidly as the critical stress is approached from above [16]. The reciprocal of this characteristic time sets a characteristic frequency at which sources will be very soft but will not bow "super-critically." For frequencies much smaller than the reciprocal of the characteristic time, the dislocation source may well produce new dislocations. For frequencies large in comparison to the reciprocal of the characteristic time, the source will not produce new dislocations.

During the portion of the cycle where the dislocation is super-critical, the effective κ is negative: The resistance that the dislocation offers to further motion is reduced with strain because the radius of the dislocation loop is increasing, and the line tension forces are consequently reduced. In addition, the line length of the dislocation, and hence the corresponding area swept out, also increases. Hence, the club shaped, non-linear hysteresis loop in figure 5 shows a negative stiffness for part of the loading cycle (the lobe of the loop). The non-linear behavior of the dislocation when over bowing occurs causes very large hysteresis losses, and explains the low frequency points deviating from the Lorentzian type loss spectrum in figures 5 and 6.

It is interesting to note that internal friction experiments frequently employ a bias stress to increase the observed signal. Typically it is argued that such bias stresses facilitate kink nucleation, and bring two nearby energy minima within range, the so-called Pare condition [14]. The results presented here suggest that there will be an additional response arising from pinned dislocation segments even in the absence of a large Peierls barrier, and kink nucleation and motion.

Dislocation Arms

The termination of the dislocation arms at the glide plane results in a significant shear stress on the glide plane that influences the dynamics of the bowing segment. (Note that there would be *no* shear component on the glide plane if the arms did not terminate.) Figure 7 shows a map of the resolved glide stress on the slip plane around an edge oriented Frank-Read source. As can be seen in the figure the arm stress field of a screw dislocation acts against the bowing of the dislocation. In this sense the glissile segment of an unbiased screw dislocation source may be thought of as a nonlinear elastic string sitting at the bottom of a potential well. The arm stresses from an edge source on the other hand, act in the opposite way, promoting bowing. Thus an edge source can be seen as an elastic string atop a potential ridge.

As the length of the pinned segment decreases, the stress field from the dislocation arms exert a greater relative influence on the dislocation dynamics. This influence leads to unusual dislocation dynamics discussed more completely below.

It should be noted that the stress topography in figure 7 is for a rectangular dislocation

normal to the slip plane (see figure 1). Such a regular loop is unlikely to be seen in real materials. Moving the arms of the loop off the normal to the slip plane changes the stress topography and, in doing so, breaks its symmetry.

Edge vs Screw

Figures 5 and 8 show that the losses associated with initially screw oriented segments are significantly lower than their edge oriented counterparts. The elastic strain energy of a screw dislocation is reduced relative to the edge dislocation by a factor of $1 - \nu$. Hence bowing the screw dislocation, so that part of it assumes edge character, requires more stress than bowing the edge segment to a partial screw orientation. As a result, a screw dislocation is intrinsically "stiffer" than an edge dislocation. This effect by itself is not sufficient to explain the large difference in stiffness between edge and screw sources. The stiffness of the dislocation source also depends on the static stress topography resulting from the stress arms. The line energy effect and the source arms act in concert to cause the relative change in stiffness from edge to screw to be much greater than $1 - \nu$.

Stress Amplitude

The loss from a linear oscillator, equation (22), has a quadratic dependence on the amplitude of the driving force. As such a parabolic rise in the peak loss with stress amplitude might be expected. Figure 8 shows the peak losses as a function of stress amplitude for edge and screw dislocation sources under 4.0MPa, 2.0MPa and no bias stresses. A parabola is fitted through the first data point in each series and extrapolated to the last. The curvature of the plots gives an indication of the effective stiffness, κ, of the sources (smaller curvatures for larger κ). The screw sources show a good agreement between the data points and the extrapolated line showing that the effective stiffness does not change much with stress amplitude. The plots for edge dislocations, on the other hand show a marked deviation from the zero amplitude stiffness. Furthermore the sign of this deviation changes with bias stress.

The trends evident in figure 8 can be explained by shape of the quasi-static stress strain curves (or stress-area curves) for a bowing dislocation sources that are shown in figure 9. The gradient of these curves give an indication of the stiffness off the sources. For an

isolated screw dislocation the stress-area curve has a negative curvature up to the critical configuration (when $\frac{d\sigma}{d\epsilon} = 0$). As a result screw source driven with a large stress amplitude will have a lower average or effective stiffness than if driven with a smaller stress amplitude. This is not the case for an edge dislocation which shows an initial stiffening as it bows, a stiffening attributable to the arm stress field. The result of increasing the stress amplitude of an unbiased edge source is initially an increase in κ. Biasing the edge source to the inflection point of the stress-strain curve gives a softening dependence of κ on the amplitude of the oscillatory shear stress. This can be seen in the direction of the deviation of the peak loss from the equilibrium stiffness peak loss in figure 8.

In all cases (including the anomalous softening), the shift in the frequencies at which the peak loses occur for different stress amplitudes, is consistent with the change in effective κ indicated by the plots in figure 8. So κ for a dislocation source is amplitude dependent.

Bias Stress

Normalised loss spectra for a 1 μm edge source driven with on oscillatory stress amplitude of 1 MPa and a variety of bias shear stresses are shown in figure 10. A static bias stress applied to a dislocation source causes the dislocation source to bow, moving the equilibrium shape of the dislocation out along the stress area curve (figure 9), and thus changing the small amplitude stiffness. For all sources, the slope of the stress area curve decreases as the critical configuration is approached. Edge oriented Frank-Read sources, however, also display an initial increase in κ as they bow. The effects of this on the peak mechanical losses of a driven source are shown in figure 11, that shows the peak losses of the normalized spectra in figure 10. This behavior is entirely consistent with equation 22 and the plots in figure 9.

Biasing the dislocation as well as changing the source stiffness, also increases the length of the glissile dislocation segment as it bows. The drag coefficient employed by the dislocation code, B, has units of Pa sec. So for a given stress the dislocation line will advance with the same speed, but the rate at which it sweeps out area will rise as the line length increases. In terms of equation (22), this is equivalent to reducing the drag, D, and so contributes a small shifts the loss spectra to higher frequencies (in addition to the shift in $\omega_{\max}$ due to the change in κ).

Near Arm Curiosity

The stress topography on the slip plane imparted by the source arms has a strong effect on the dynamics of the dislocation and ignoring the stress from the arms drastically changes the loss spectrum. As the dislocation is in the damped limit, and the dynamics are inherently non-equilibrium, the section of dislocation near the arms lead as the dislocation bows out (the mobile segment is "m" shaped as shown in figure 4). Under certain low-stress and high-frequency conditions, the arm-stress can cause an unbiased dislocation to become trapped in a slightly bowed configuration, where the near arm segments stay to one side of the equilibrium line through out the whole cycle. In this regime, the centroid of the hysteresis loop moves away from the origin. The direction of the shift is determined by the initial sign of the applied stress. In this case, the center of the hysteresis loop is shifted away from the origin along the area axis.

V. Elastically Interacting Dislocations

Experimental observations of post deformation microstructures reveal a complex dislocation cell structure, in which most of the dislocations are bound in cell walls [19–22]. Hence, when one is interpreting internal friction measurements one should consider the losses from the collective response of cell walls, rather than the response of isolated dislocations. To the current knowledge of the authors, there exist no predictions of the mechanical losses arising from application of oscillatory stress to a cell boundary.

The simulations of the dynamics of elastically interacting dislocation sources under oscillatory loads described in this section are a (very!) modest first step towards understanding the dynamic response of cell boundaries. Simple configurations of two edge or screw dislocations are used. These consist of two sources, vertically stacked such that the mobile segments are adjacent to each other, and have the same line direction and burgers vector. A diagram of these stacked configurations is shown in figure 12. The respective glide planes of the two sources are separated by a height h. If the glissile segments are initially screw-oriented, they repel each other until the repulsion is opposed by the self stress (figure 12.b). Consequently, even in the absence of an externally applied stress, the mobile segments are bowed at equilibrium. (This is a reasonable result as boundaries composed of a single type

of screw dislocation have infinite energy and are inherently unstable.)

In the initially edge-oriented case, at equilibrium the mobile segments lie on top of each other and the dislocations stay "locked" together as they bow under an applied load (figure 12a). However, if h, the separation between the glide planes of the edge structure, is sufficiently small, another locally stable configuration is possible. The shear stress generated by an edge dislocation changes sign as one traverses a plane parallel to the slip plane. As a result, two edge dislocations bowed to sufficiently different extents will experience a repulsive force between the apex of their bowed segments. This can result in an "unlocked" configuration, similar to the screw stack. Figure 12c shows such an unlocked edge stack at local equilibrium under a 4.0 MPa static biasing stress.

Figure 13 shows the loss spectrum (measured per dislocation) for isolated and stacked screw sources. There is a slight drop in the peak energy loss per dislocation based on expectations from an isolated source. There is also a shift to higher freqencies. At first glance, this unusual behavior is counterintuitive. The screw sources repel each other effectively applying a positive and negative bias stress on each other (*i. e.* the stack is "self-biasing"). This would lead one to expect interacting screw dislocations to soften with respect to an isolated screw source, yielding an increased loss, according to equation 22. However, the quasi-static stress strain curve in figure 9 shows that the stacked screw dislocations are marginally stiffer than isolated screw sources. More importantly, the geometry of the studied configuration has now two sets of dislocation arms terminating at glide planes. The line direction in each of the sources is such that the stress field from the two two sets of arms act in the same way. The arm stress field of screw sources acts to stiffen them, and this extra arm stress causes the slightly highter stiffness of the intereacting self biased boundary. This increased line length of the self bowing segments acounts for the extra shift in frequency of the peak loss.

Figure 9 can also be used to understand the mechanical losses of the stacked edge dislocation structures that appear in figures 14 and 15 (with respect to an isolated edge Frank-Read source). An interesting feature of the stress vs area curves for the multidislocation structures is that they may terminate before the gradient goes to zero, as one dislocation may go super-critical before the other. The increased stress topography on the glide plane of the stacked structures should act to soften the edge dislocation structures. However, the elastic interactions between the mobile segments must also be considered. In the case of

the locked edge dislocations the elastic interaction between distant parts of the two bowing dislocations is attractive. The interaction between the part of the line in vertical alignment is very small. This effectively increases the far field contribution to the self stress of the bowed dislocation, and stiffens the bowed dislocation.

The unlocked edge stack is self biasing, like the screw stack, but the bowing segments are self biased to the stiff region of the stress strain curve. Again there is a small shift in frequency attributed to the drop in the effective drag, D. The stress area curve of the unlocked edge sources display softening at around 4.0 MPa and so biasing an unlocked stack causes the energy losses to rise above those for a similarly biased isolated source. This can be seen in figure 15.

Finally, it is noted that the values of h employed here are characteristic of a $\sim 0.5^\circ$ tilt boundary. Hence it seems quite likely that modeling the response of higher angle boundaries requires consideration of the many dislocation problem.

VI. CONCLUSIONS

The work presented here explores the dislocation dynamics predicted by a front tracking algorithm for dislocation dynamics. In particular, the mechanical losses expected from applying an oscillatory load to various configurations of Frank-Read sources are considered.

It is first demonstrated, by comparison with the exact solution of the small stress amplitude limit, that the dislocation dynamics code applied here gives an excellent description of the mechanical losses in the limit of large core cutoff. This test, while not a test of general conditions, does provide some confidence that the simulations are producing reasonable results. Bouyed by this confidence, the dislocation dynamics code is then used to explore losses under more realistic conditions.

The current work considers two situations: isolated Frank-Read sources, and stacked Frank-Read sources. At high frequencies, the isolated Frank-Read sources behaved as expected from the Granato-Lücke model for mechanical losses. The sources display an increased maximum loss occuring at a lower frequency than that predicted by Granato-Lücke theory. Adjusting the line tension of the Granato-Lücke model (which is effectively the procedure one would apply in the analysis of an experiment) can lead to better agreement between the model and the simulation for the amplitude of the losses, but the Granato-Lücke

model still overestimates the frequency at which one observes the maximum loss.

Under an applied bias stress such that the amplitude of the bias stress and the oscillatory stress exceeds the critical stress for operation of the Frank-Read source, the frequency dependence of the loss deviates substantially from a simple Lorentzian shape. Instead, the former maximum in the loss becomes a local maximum in the loss vs frequency plot. Further, the application of a bias stress can increase the losses associated with the dislocation substantially. The deviation is clearly evident in the dislocation hysteresis loops, which switch from an elliptical shape to that resembling a golf club. This deviation is particularly important to experiment, as internal friction measurements are often done under an applied bias load to increase the signal.

It is also noted that in experimental situations, the dislocations responsible for the losses are often contained within dislocation boundaries. Hence, it is reasonable to consider the effects of these boundaries on the expected losses. As the starting point for such an investigation, the current paper considers the interaction between two Frank-Read sources. It is shown that dislocation interactions may alter substantially the losses expected from the dislocations (as compared with the simple sum of noninteracting dislocations).

VII. Acknowledgment

The authors gratefully acknowledge support from the Department of Energy through the Basic Energy Sciences Division of the Office of Science under contract No. DE-AC03-76SF00098.

VIII. Appendix

The self-stress of a dislocation is given by [18]

$$\begin{aligned} \boldsymbol{S}(\boldsymbol{r}) &= \frac{\mu}{4\pi}\oint_{\text{line}}\left\{(\boldsymbol{b}\times\boldsymbol{\nabla}')\frac{1}{R}\otimes d\boldsymbol{l}'\right\} \\ &+ \frac{\mu}{4\pi}\oint_{\text{line}}\left\{d\boldsymbol{l}'\otimes(\boldsymbol{b}\times\boldsymbol{\nabla}')\frac{1}{R} - \boldsymbol{\nabla}'\cdot\boldsymbol{b}\times d\boldsymbol{l}')(\boldsymbol{\nabla}\times\boldsymbol{\nabla} - \boldsymbol{I}\boldsymbol{\nabla}^2)\frac{R}{(1-\nu)}\right\}, \end{aligned} \tag{23}$$

where ν is Poisson's ratio, $d\boldsymbol{l}' = \boldsymbol{\xi}(\boldsymbol{r}')|dl'|$ (where dl is an incremental distance along the line) and $R = |\boldsymbol{r}' - \boldsymbol{r}|$. The resulting Peach-Koehler force felt by the dislocation is

$$\boldsymbol{F}_{\text{self}}(\boldsymbol{r}) = (\boldsymbol{S}(\boldsymbol{r}) \cdot \boldsymbol{b}) \times \boldsymbol{\xi}(\boldsymbol{r}). \tag{24}$$

Pinning the ends of the mobile dislocation segment at the origin and $\boldsymbol{r} = (L, 0, 0)$, and confining it to glide with small amplitude oscillations on the $z = 0$ plane, gives $\boldsymbol{r}(t) = (x, y(x,t), 0)$ and allows the unknown function $y(x,t)$ to represented as a sine Fourier series

$$y(x,t) = \sum_{\substack{n=1 \\ n\,\text{odd}}}^{\infty} a_n(t) \sin\left(\frac{xn\pi}{L}\right). \tag{25}$$

Taylor expanding the self-glide force in the coefficients $\{a_n\}$ about the unbowed configuration and only retaining terms up to first order in $\{a_n\}$ gives a sum of force distribution functions for each of the vibrational modes

$$\boldsymbol{F}_{\text{self}}(\boldsymbol{r}) \approx \sum_{\substack{n=1 \\ n\,\text{odd}}}^{\infty} \frac{\partial}{\partial a_n} \left((\boldsymbol{S}(\boldsymbol{r}) \cdot \boldsymbol{b}) \times \boldsymbol{\xi}(\boldsymbol{r})\right) \Big|_{\{a_n\}=0} a_n(t) = \sum_{\substack{n=1 \\ n\,\text{odd}}}^{\infty} a_n(t) f_n(x). \tag{26}$$

The force distribution functions are given by the line integral

$$\begin{aligned} f_n(x) = &\int_0^{x-\rho} \frac{b_y^2 \mu}{4\pi} \left(\frac{n\pi(x'-x)\cos\left(\frac{nx'\pi}{L}\right)}{L|x'-x|^3} + \frac{\sin\left(\frac{nx\pi}{L}\right) - \sin\left(\frac{nx'\pi}{L}\right)}{|x'-x|^3\,(1-\nu)} \right) dx' \\ &+ \int_{x+\rho}^{L} \frac{b_y^2 \mu}{4\pi} \left(\frac{n\pi(x'-x)\cos\left(\frac{nx'\pi}{L}\right)}{L|x'-x|^3} + \frac{\sin\left(\frac{nx\pi}{L}\right) - \sin\left(\frac{nx'\pi}{L}\right)}{|x'-x|^3\,(1-\nu)} \right) dx'. \end{aligned} \tag{27}$$

(If the point in question is nearer to a corner than ρ, only the appropriate term is retained.) For a general point, integrating yields the expression

$$\begin{aligned} f_n(x) = &\tau \left(\frac{\kappa L}{2x\tilde{x}}\,(1-2\nu) - \sin(\kappa x) \frac{L^2 - 2Lx + 2x^2}{2\tilde{x}^2 x^2} \right) \\ &+ \tau \frac{\sin(\kappa x)}{\rho^2}\,(1 - \cos(\kappa\rho) - \kappa\rho(1-2\nu)\sin(\kappa\rho)) \\ &+ \tau\kappa^2(1-2\nu)\cos(\kappa x) \left(\frac{\text{si}(\kappa x) - \text{si}(\kappa\tilde{x})}{2} \right) \\ &- \tau\kappa^2(1-2\nu)\sin(\kappa x) \left(\frac{\text{ci}(\kappa\tilde{x}) + \text{ci}(\kappa x)}{2} - \text{ci}(\kappa\rho) \right), \end{aligned} \tag{28}$$

where

$$\tilde{x} = L - x, \tag{29}$$

$$\kappa = \frac{n\pi}{L}, \tag{30}$$

$$\tau = \frac{b_y^2 \mu}{4\pi\,(1-\nu)}, \tag{31}$$

$$\tag{32}$$

and $\mathrm{si}(x)$ and $\mathrm{ci}(x)$ are the sine and cosine integrals of x respectively.

---

[1] Y. U. Wang, Y. M. Jin, A. M. C. No, and A. G. Khachaturyan, Acta Materialia **49**, 1847 (2001).

[2] M. Rhee, H. M. Zbib, J. P. Hirth, H. Huang, and T. de la Rubia, Modelling and Simulation in Materials Science and Engineering **6**, 467 (1998).

[3] N. M. Ghoniem and R. Amodeo, in *Diffusion and Defect Data - Solid State Data, Part B* (International C.N.R.S. Meeting on Non Linear Phenomena in Materials Science, Aussois, France, 1988), vol. B3-B4 of *Solid State Phenomena*, p. 377.

[4] M. Rhee, D. H. Lassila, V. V. Bulatov, L. Hsiung, and T. D. de la Rubia, Philosiphical Magizine Letters **81**, 595 (2001).

[5] L. K. Wickham, K. W. Schwarz, and J. S. Stölken, Physical Review Letters **83**, 4574 (1999).

[6] K. W. Schwarz, Journal of Applied Physics **85**, 108 (1999).

[7] K. W. Schwarz, Journal of Applied Physics **85**, 120 (1999).

[8] N. M. Ghoniem, in *Porceedings of the 1st Latin American Summer School on Materials Instabilities* (Kluwer, 1998).

[9] A. N. Gulluoglu, D. J. Srolovits, R. LeSar, and P. S. Lomdahl, Scripta Metallurgica **23**, 1347 (1989).

[10] S. Swaminarayan and R. LeSar, Computational Materials Science **21**, 339 (2001).

[11] K. W. Schwarz and F. K. LeGoues, Physical Review Letters **79**, 1877 (1997).

[12] L. Kubin, G. Canova, M. Condat, B. Devincre, V. Pontikis, and Y. Brechet, Solid State Phenomena **23-24**, 455 (1992).

[13] M. Tang, L. P. Kubin, and G. R. Canova, Acta Materialia **46**, 3221 (1998).

[14] G. Fantozzi, C. Esnouf, W. Benoit, and I. G. Richie, Progress in Materials Science **27**, 311 (1982).

[15] A. Granato and K. Lücke, J. Appl. Phys. **27**, 583 (1956).

[16] A. K. Faradjian, L. H. Friedman, and D. C. Chrzan, Modelling Simul. Mater. Sci. Eng. **7**, 479 (1999).

[17] P. A. Greaney and D. C. Chrzan, in *Multiscale Phenomena in Materials - Experiments and Modeling Symposium*, edited by I. M. Robertson, D. H. Lassila, B. Devincre, and R. Phillips

(Materials Research Society, Boston, MA, USA., 1999), vol. 578, pp. 161–6.

[18] J. P. Hirth and J. Lothe, *Theory of Dislocations* (Krieger Publishing Company, Malabar, Florida, 1992), 2nd ed.

[19] B. Bay, N. Hansen, and D. Kuhlmann-Wilsdorf, Mater. Sci. Eng. **A113**, 385 (1989).

[20] D. Kuhlmann-Wilsdorf and N. Hansen, Metall. Trans. A. **20**, 2393 (1989).

[21] N. Hansen, Mater. Sci. Technol. **7**, 1039 (1990).

[22] B. Bay, N. Hansen, D. A. Hughes, and D. Kuhlmann-Wilsdorf, Acta metall. mater. **40**, 205 (1992).

[23] While not the only possible choice, this is the most convenient for the present simulations.

[24] In the present work it is meaningless to discuss a quality factor, as there are a finite number of dislocations embedded in an infinite medium.

[25] All terms in equation (20) where $n \leq 19$ and $m \leq 19$.

[26] Over the range of frequencies ploted here the loss calculated by Granato-Lücke theory, which accounts for the dislocation mass, is indistinguishable from the loss of a massless vibrating string. As such the massless dislocation approximation employed by the dislocation code, and the Fourier series calculation, is valid over this frequency range

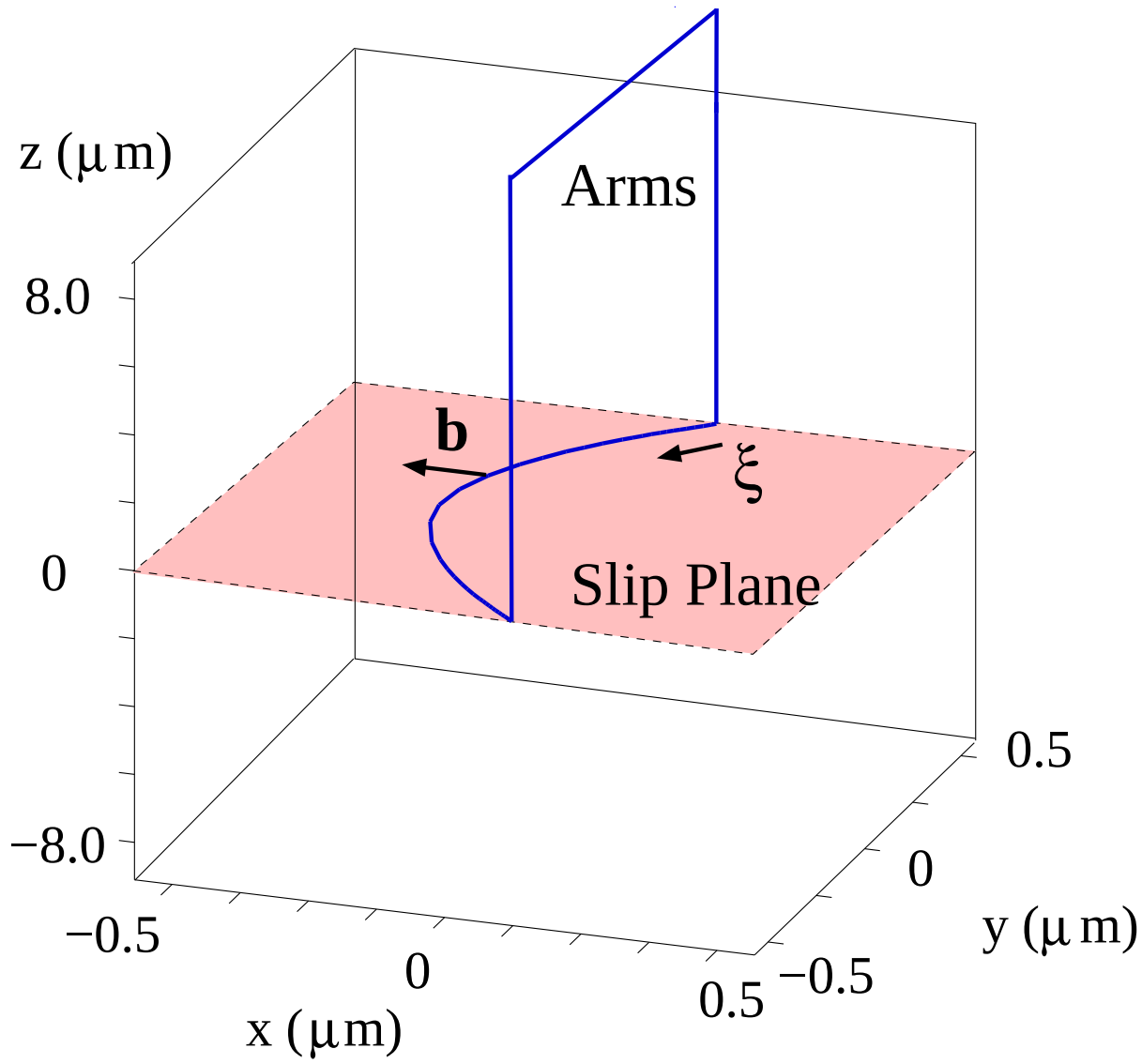

FIG. 1: An edge oriented Frank-Read source.

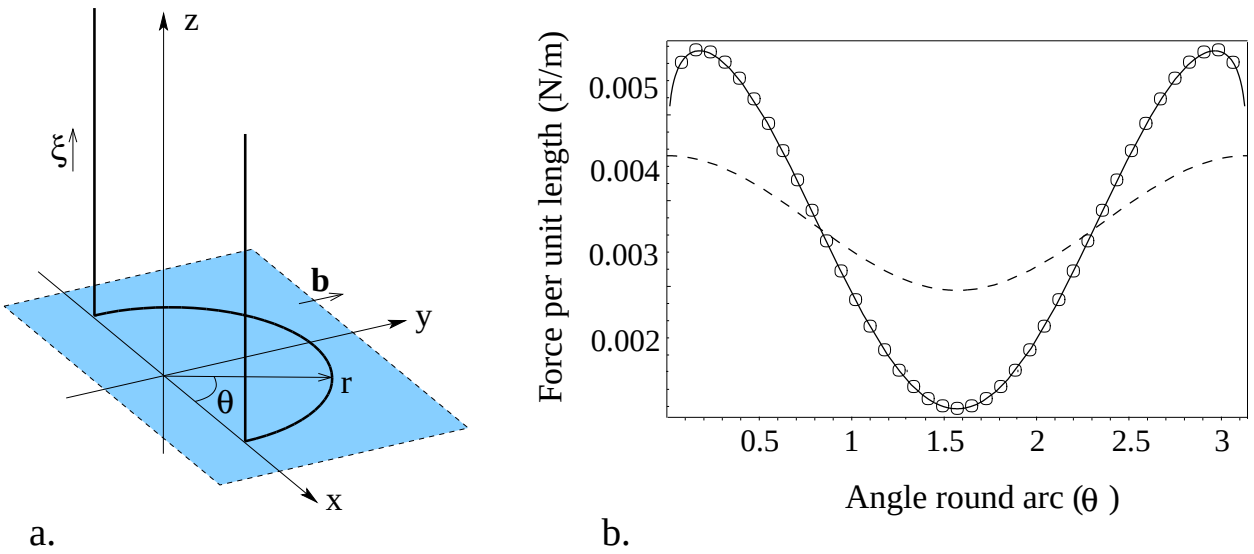

FIG. 2: Test configuration: a) shows a 1 μm artificially semi-circularly bowed, edge oriented, dislocation source, b) shows the magnitude of the self force as a function of angle round the bowed arc calculated using the numerical scheme (circles), the analytic solution (solid line), and using straight line tension approximation (dashed). The agreement between the exact result and the predictions of the computer model is excellent.

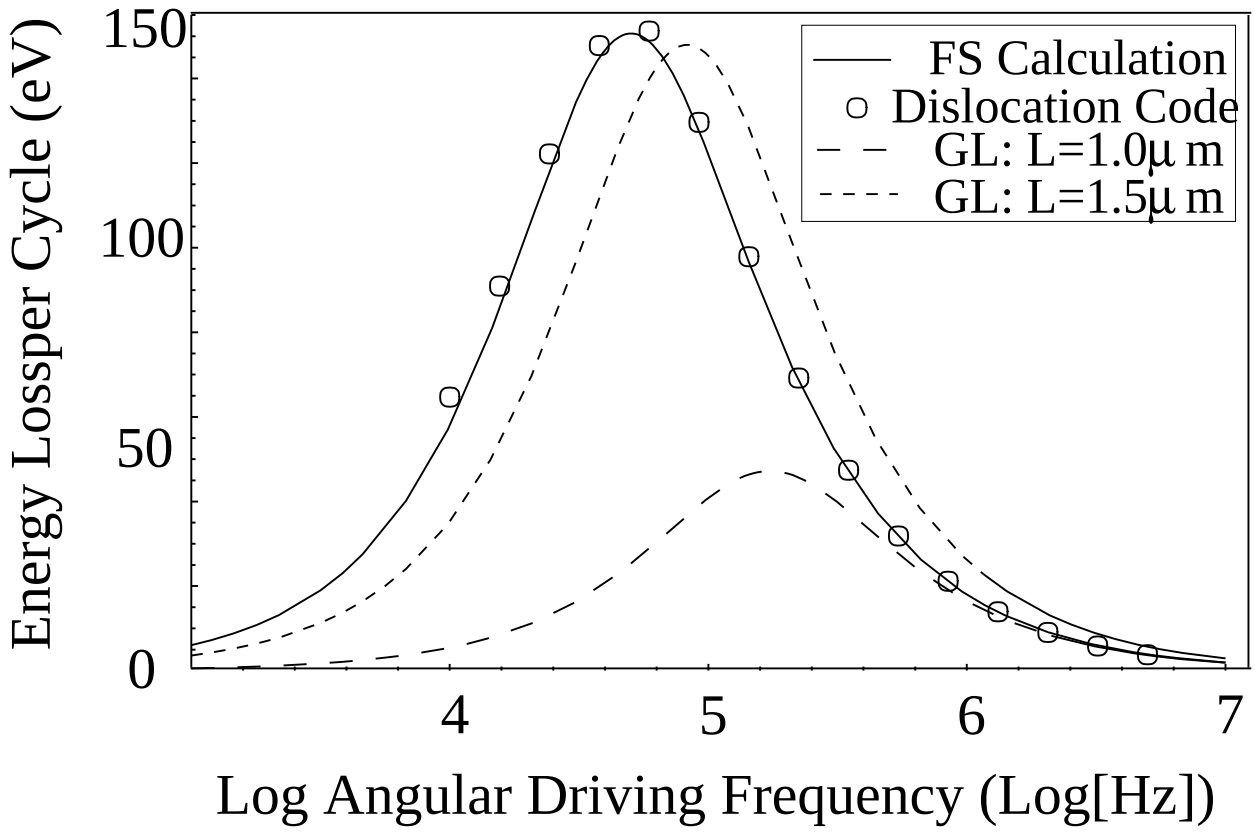

FIG. 3: Loss spectra for a 1 μm edge oriented Frank-Read source, under no bias stress and driven with a 0.5 MPa sinusoidal stress. The spectra are calculated using the truncated Fourier series (solid), the dislocation code (circles), and the theory of Granato and Lücke (short-dashed) [15]. The long-dashed line was also calculated using Granato-Lücke theory but for a 1.50 μm Frank-Read source. In all cases dislocation arms were ignored and an abnormally large cutoff ($\rho = 5 \times 10^{-9}$m) was assumed. The statistical errors in the simulations are smaller than the displayed symbols.

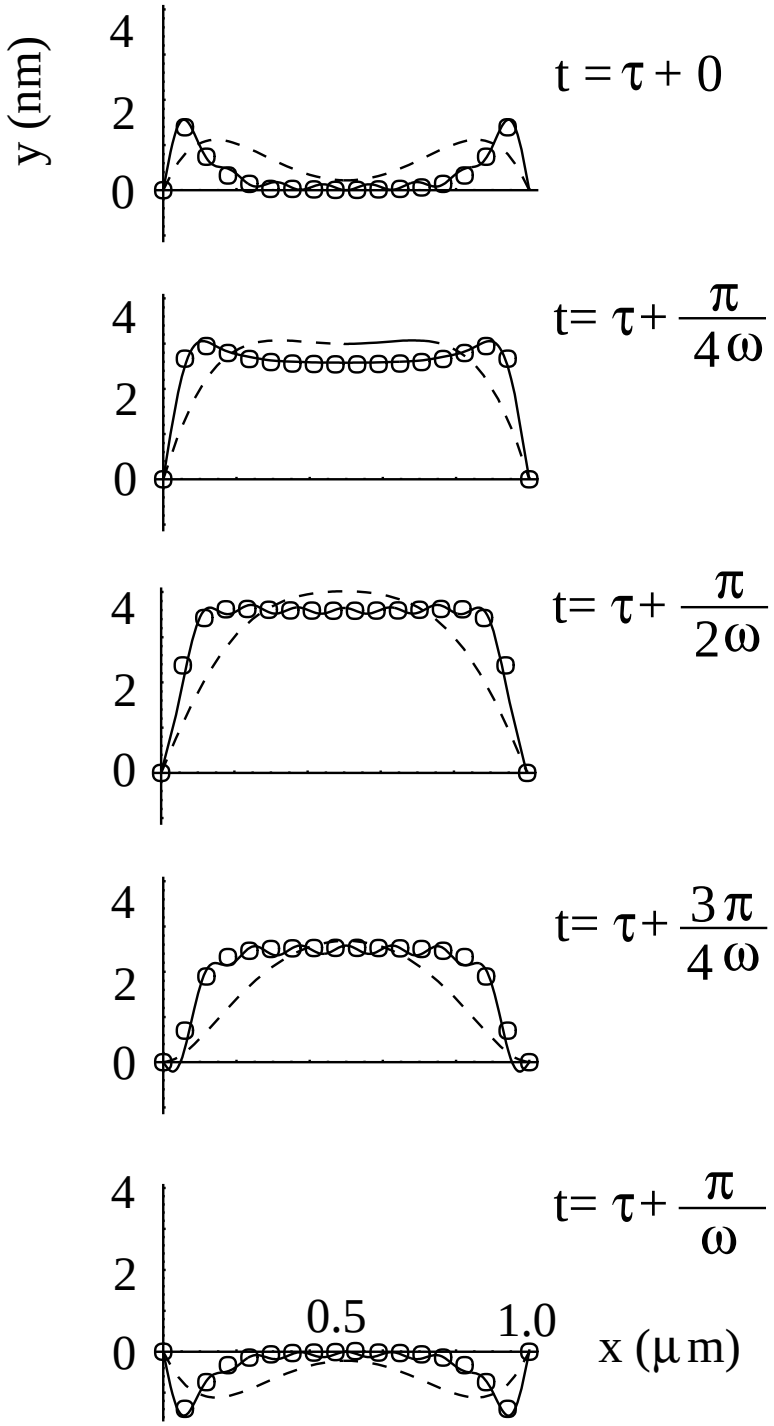

FIG. 4: Bowing configurations of steady state oscillation at 1 MHz calculated using the dislocation code (circles), the first 8 terms of Fourier series method (solid), and the method of Granato-Lücke (again with the first 8 terms). Calculations use an inner cutoff $\rho = 50$ Å, and the arm stress in ignored.

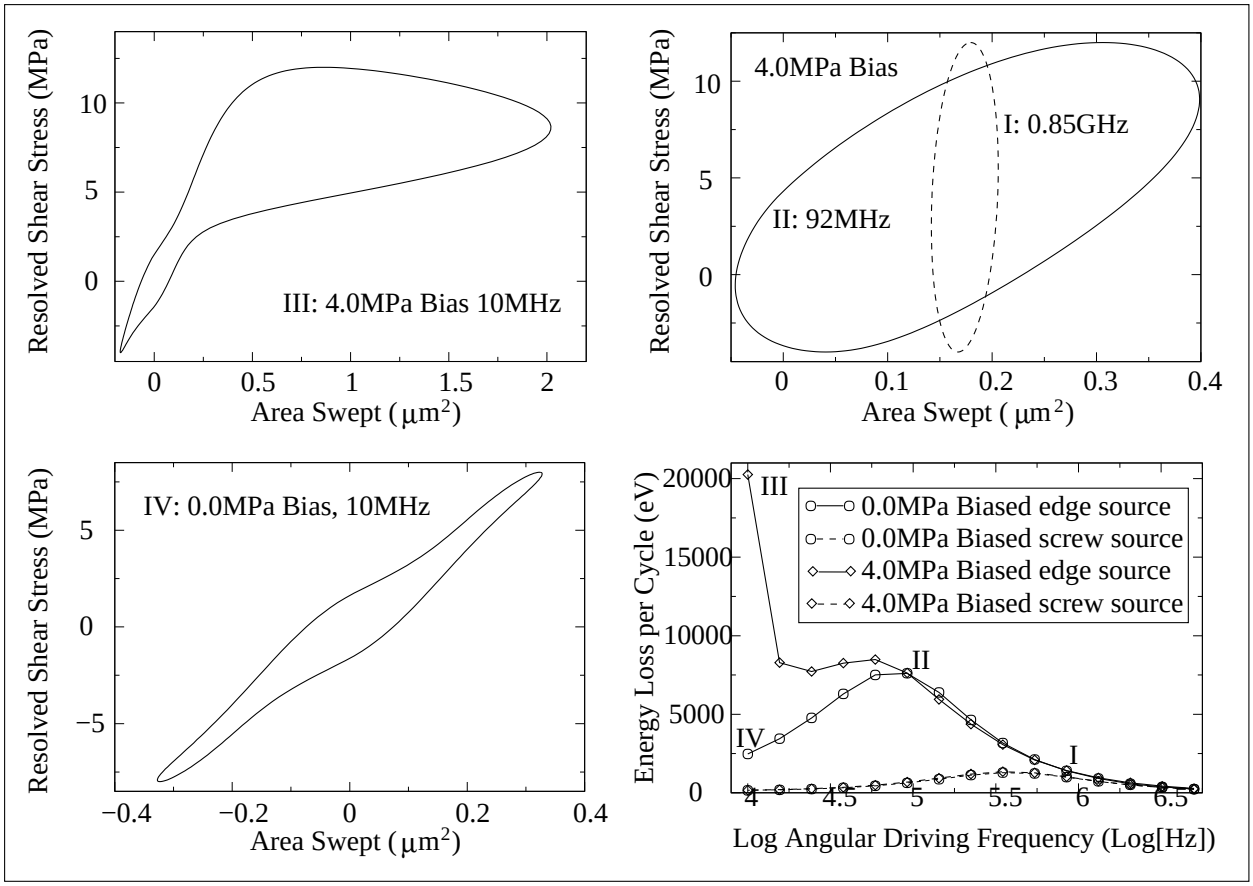

FIG. 5: Loss spectra and hysteresis loops for 1 μm edge and screw Frank-Read sources, under 4.0 MPa and zero bias stresses and driven with an 8.0 MPa amplitude oscillatory stress.

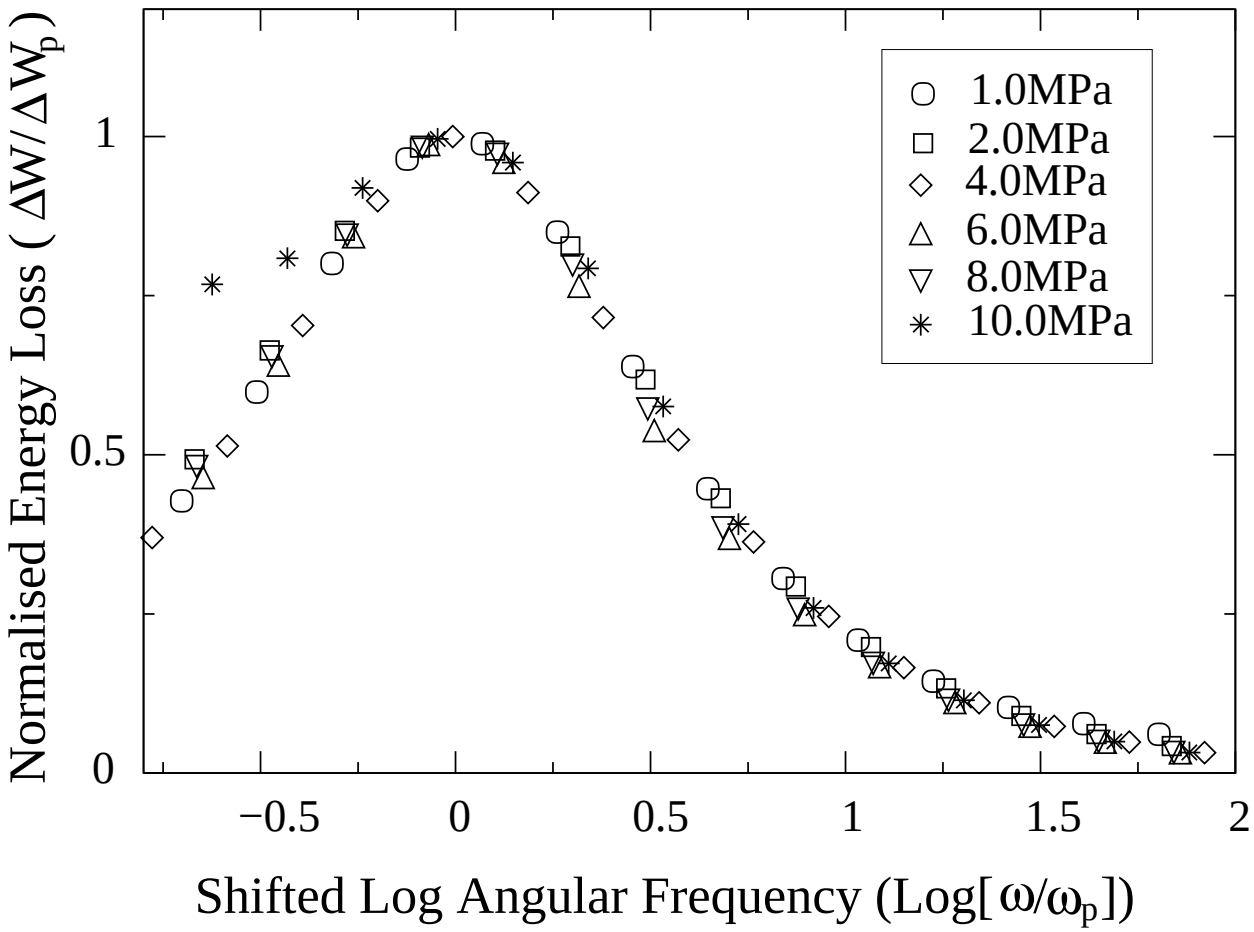

FIG. 6: Normalized loss spectra for unbiased, 1 μm, isolated, edge Frank-Read sources, driven with different oscillatory shear stress amplitudes.

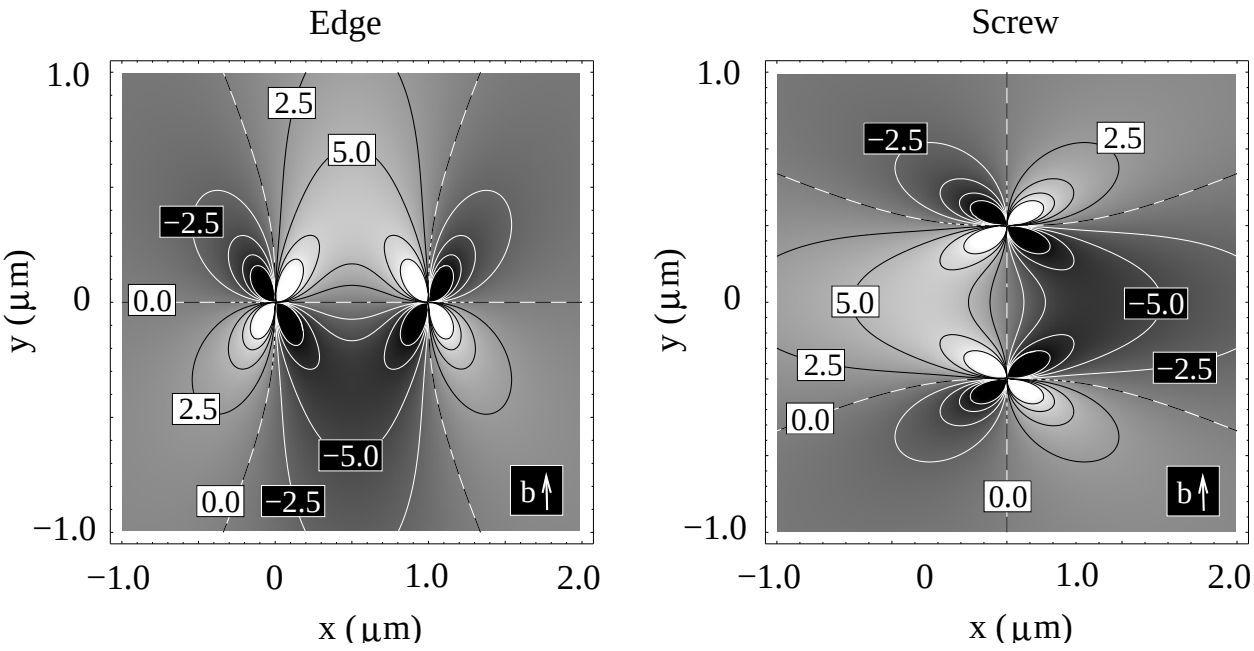

FIG. 7: Contour map of the resolved glide force on the slip plane for edge and screw oriented sources. Contours are in units of 10 mN cm^{-1} and are spaced in intervals of 25 mN cm^{-1}. White contours indicate negative forces and black contours positive forces.

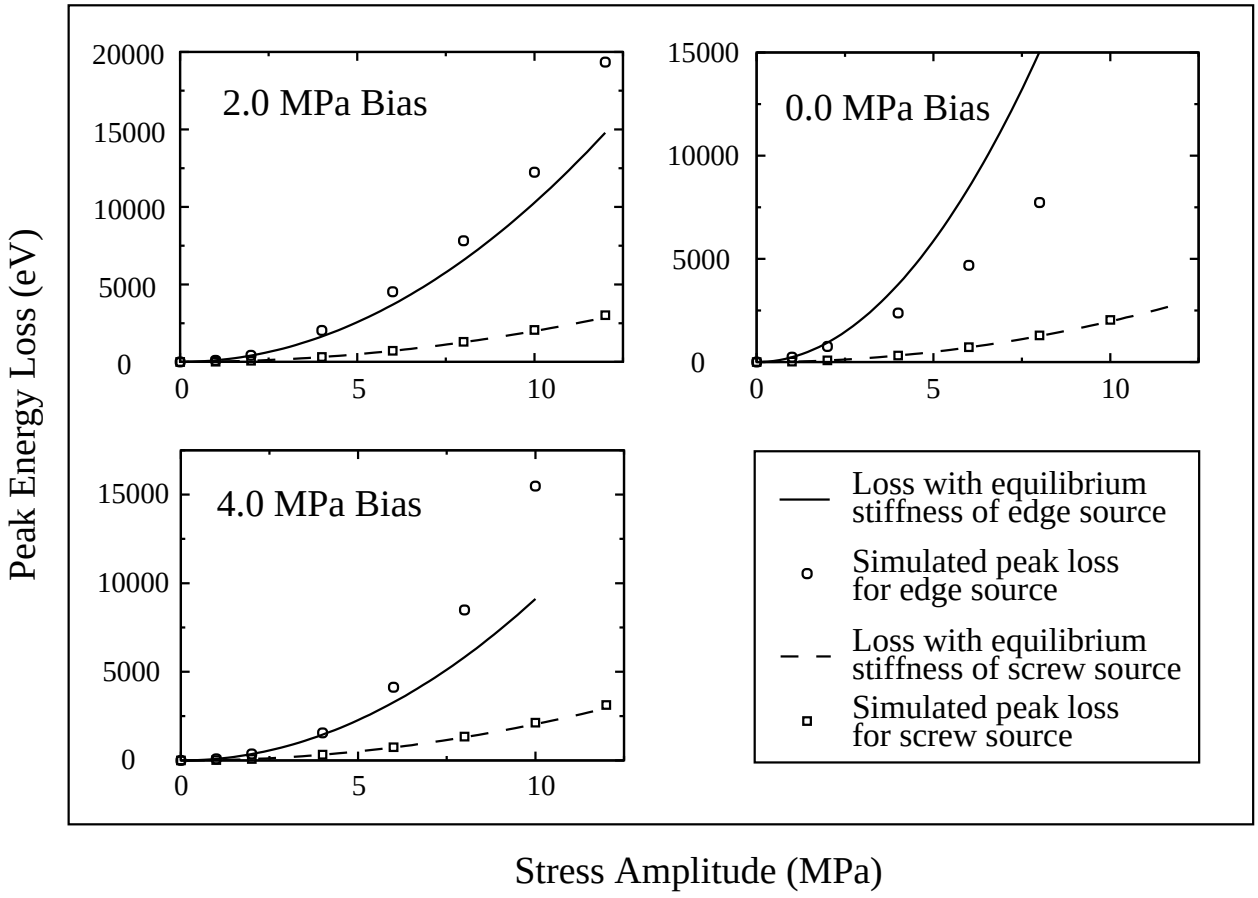

FIG. 8: Change in peak loss vs oscillatory driving stress amplitude for differing bias stresses. See text for details.

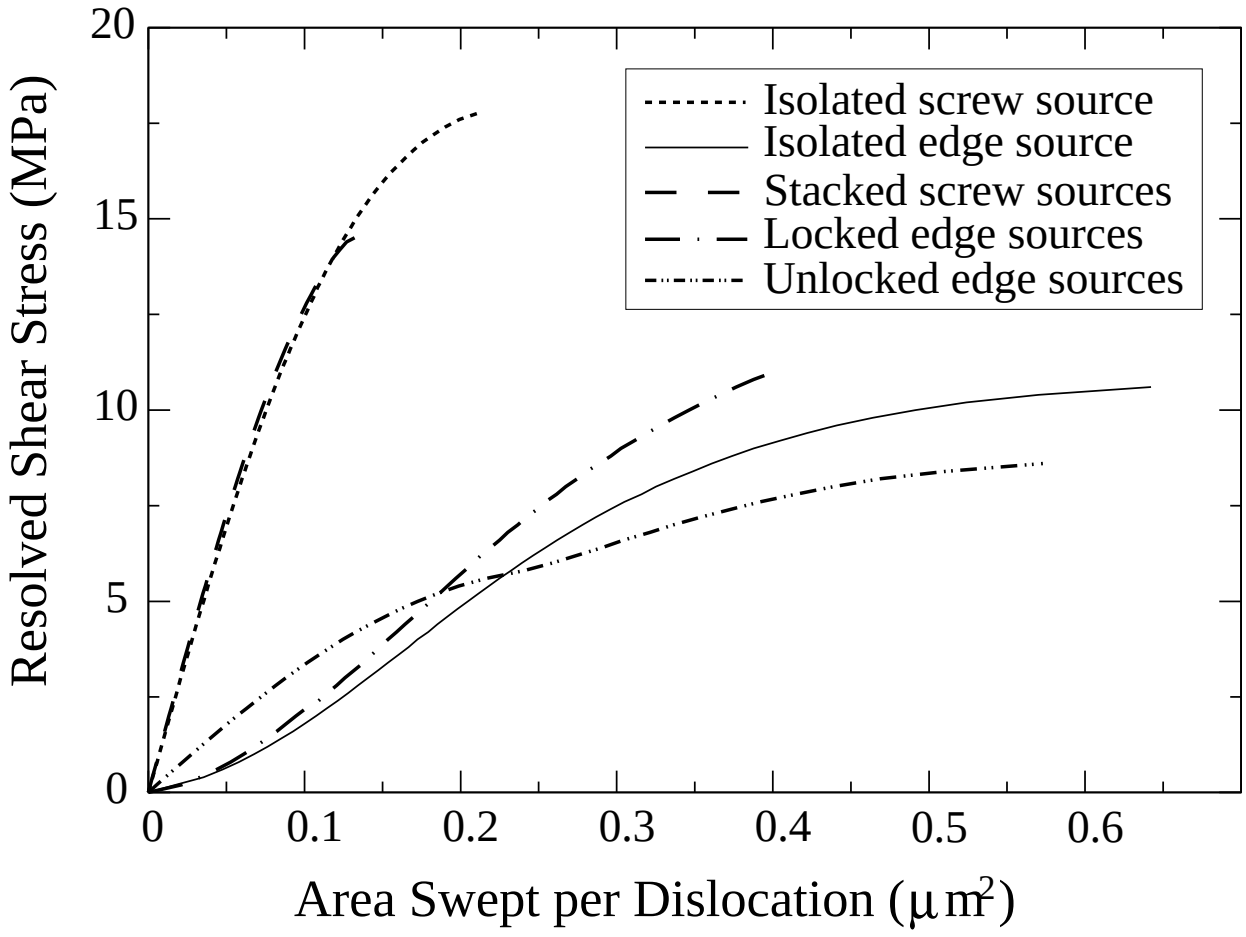

FIG. 9: The quasi-static plot of area swept versus applied static stress for a 1 μm source.

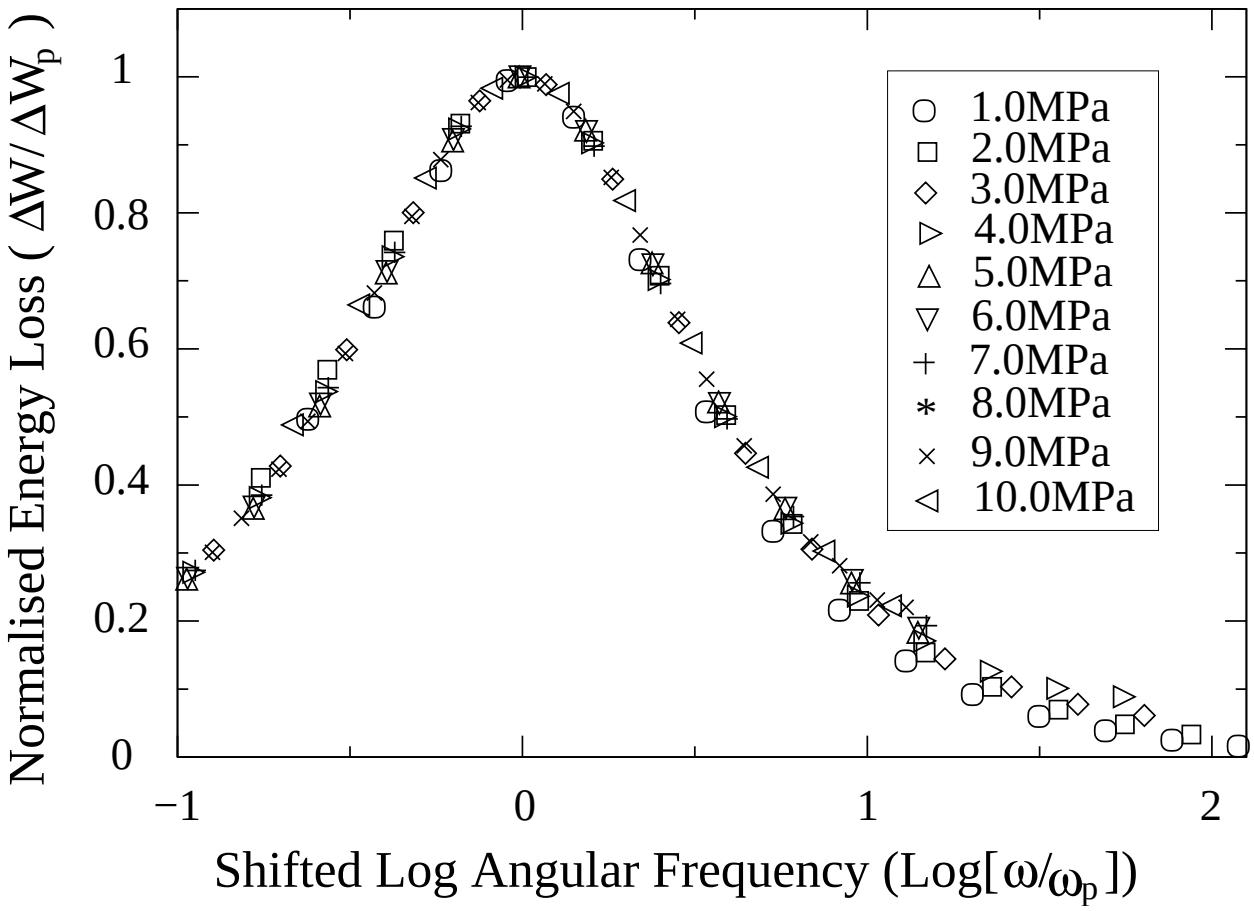

FIG. 10: Normalised loss spectra for 1μm, isolated, edge Frank-Read sources, driven with σ_a = 1.0MPa, for different biases.

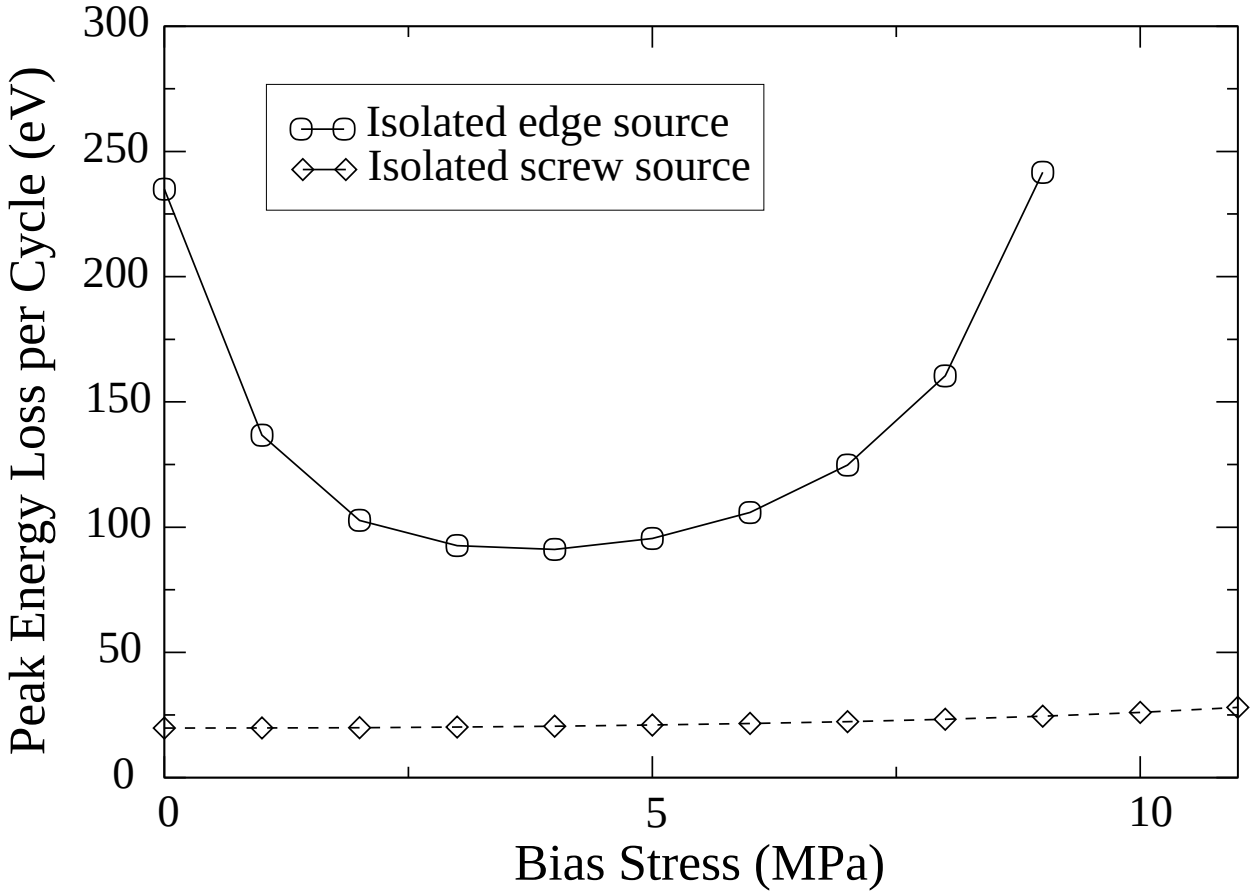

FIG. 11: Peak energy loss for isolated 1 μm, edge and screw sources driven with a 1.0 MPa oscillatory shear stress under different bias stresses.

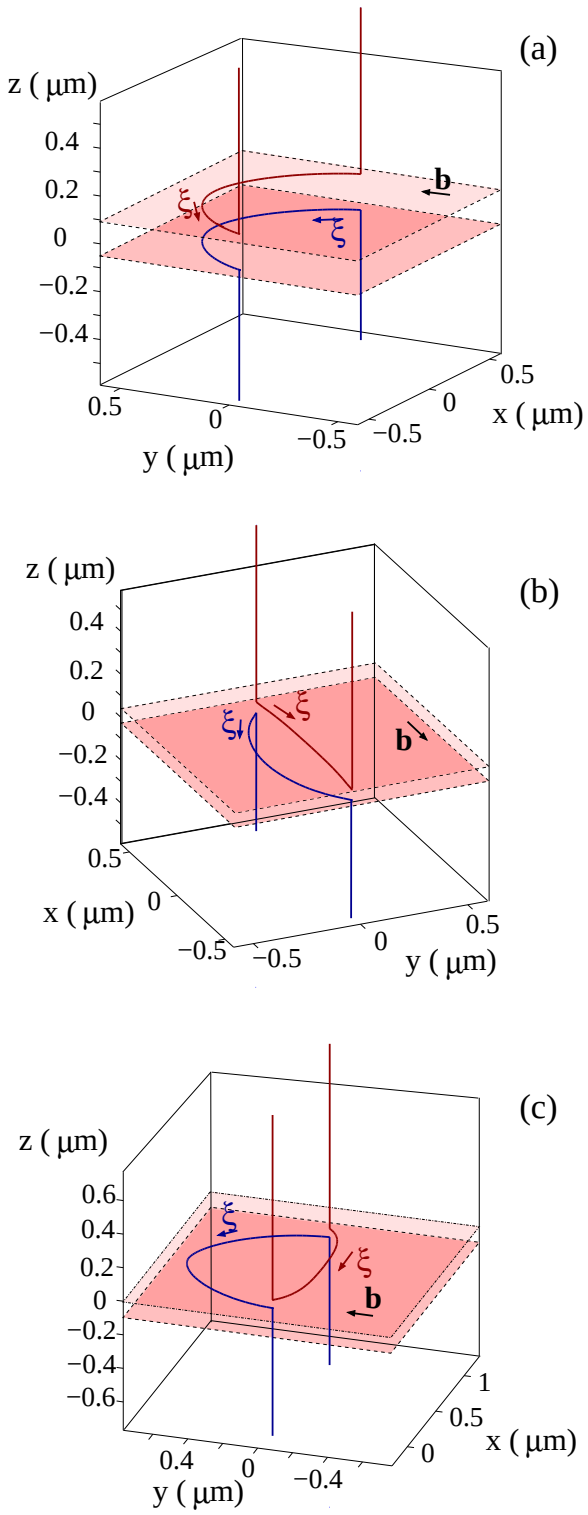

FIG. 12: Configurations of locked stacked edge sources (a), stacked screw sources (b) and unlocked stacked edge sources (c), all under a static bias stress.

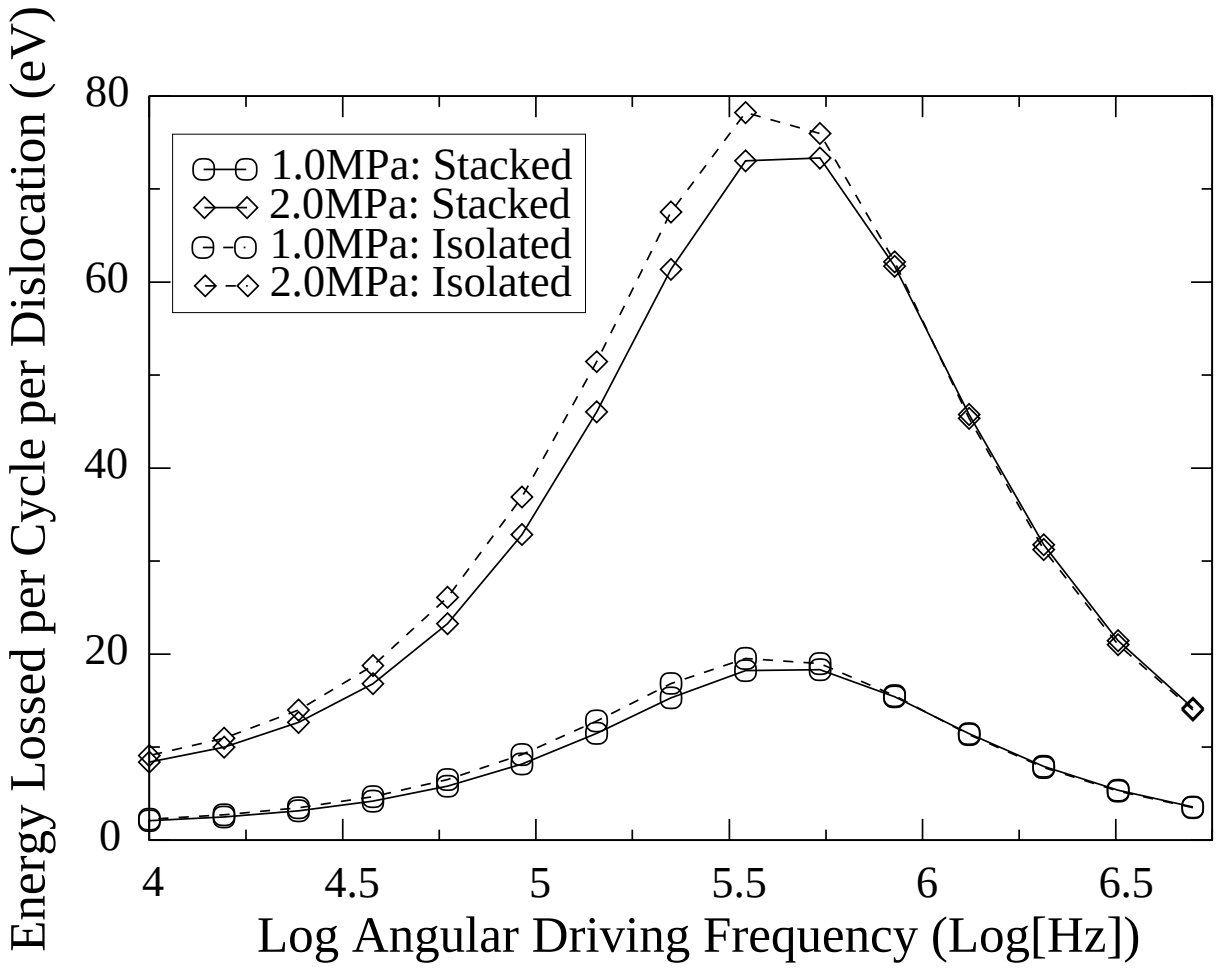

FIG. 13: Loss spectra of unbiased isolated and stacked 1 μm screw sources driven with 1.0 MPa and 2.0 MPa stress amplitudes.

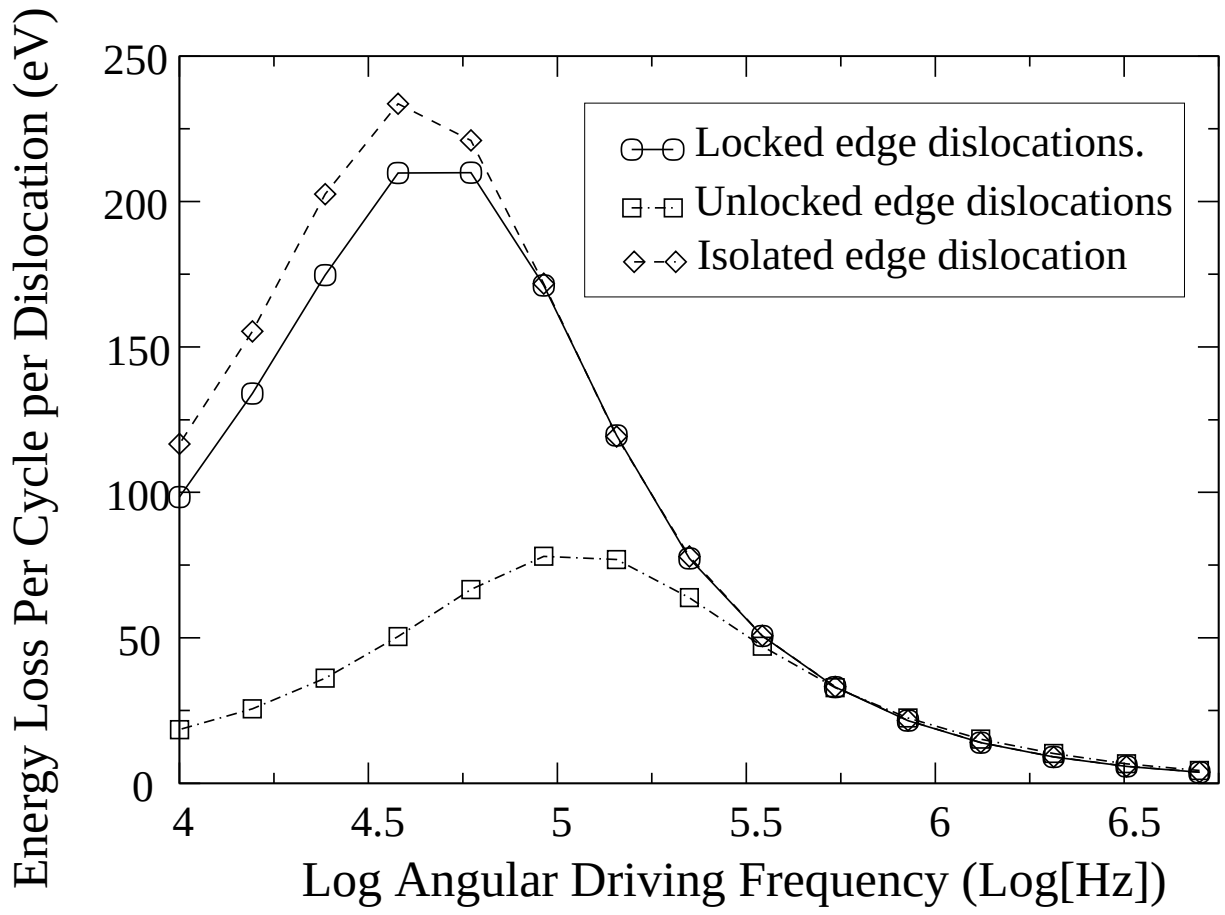

FIG. 14: Loss spectra for unbiased, locked, unlocked and isolated 1 μm edge Frank-Read sources.

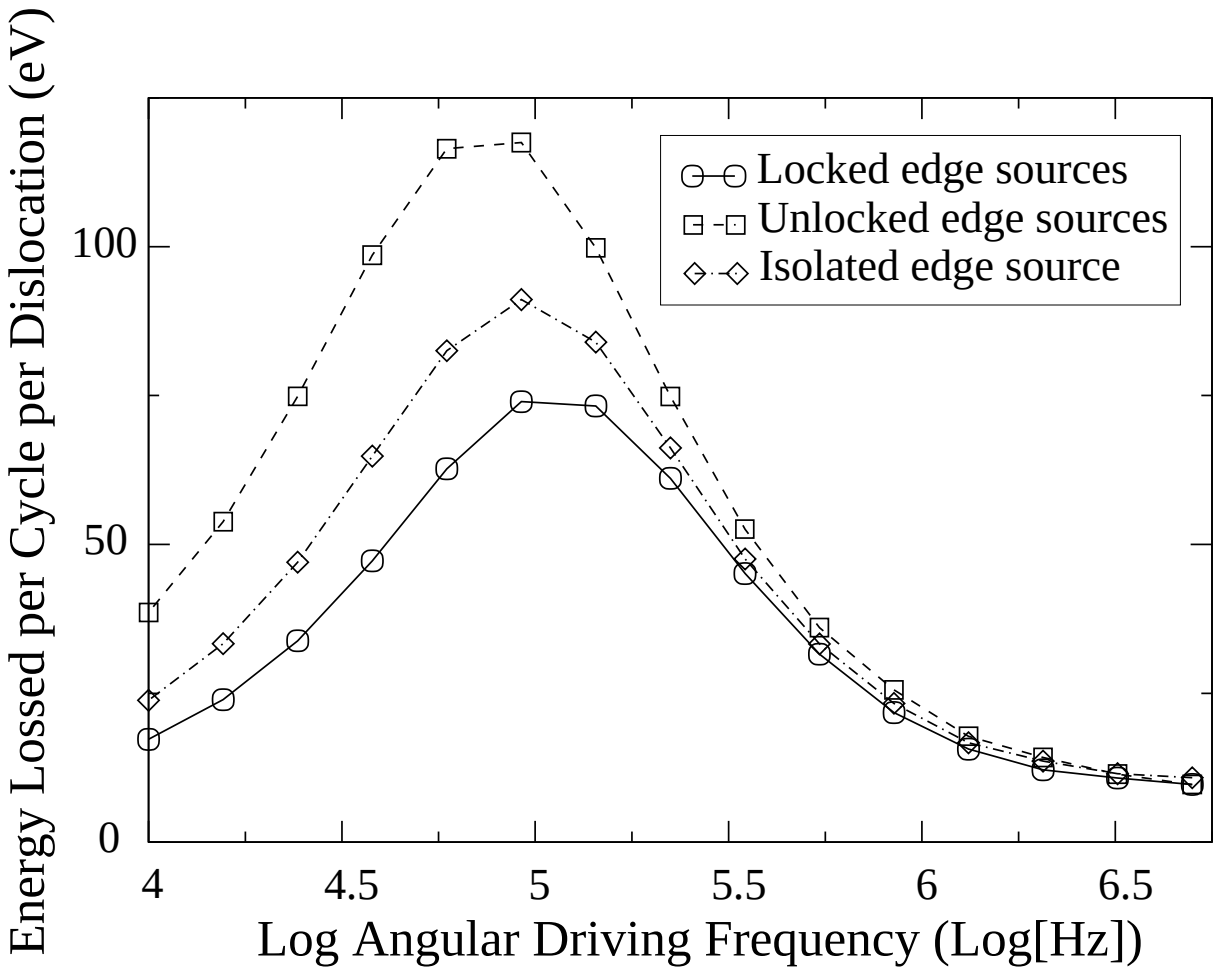

FIG. 15: Loss spectra for 4.0 MPa biased, locked, unlocked and isolated 1 μm edge Frank-Read sources.